

Communication

Effect of Structure-Controlled Ruthenium Oxide by Nanocasting in Electrocatalytic Oxygen and Chlorine Evolution Reactions in Acidic Conditions

Jisu Han ^{1,2}, Hyung Jun An ¹, Tae-Wan Kim ^{1,3}, Kwan-Young Lee ², Hyung Ju Kim ^{1,3}, Youngmin Kim ^{1,*}  and Ho-Jeong Chae ^{1,3,*}

¹ Carbon Resources Institute, Korea Research Institute of Chemical Technology, Daejeon 34114, Korea; jisuhan@kRICT.re.kr (J.H.); ahj8228@kRICT.re.kr (H.J.A.); twkim@kRICT.re.kr (T.-W.K.); hjkim@kRICT.re.kr (H.J.K.)

² Department of Chemical and Biological Engineering, Korea University, Seoul 02841, Korea; kylee@korea.ac.kr

³ Advanced Materials and Chemical Engineering, University of Science and Technology, Daejeon 34113, Korea

* Correspondence: ykim@kRICT.re.kr (Y.K.); hjchae@kRICT.re.kr (H.-J.C.); Tel.: +82-42-610-8576 (Y.K.); +82-42-860-7290 (H.-J.C.)

Received: 31 May 2019; Accepted: 17 June 2019; Published: 19 June 2019



Abstract: RuO₂ has been used for various applications because of its good catalytic properties. To further improve its electrocatalytic properties, we used a nanocasting technique. By using this technique, we obtained structure-controlled (SC) RuO₂ with a high surface area and an ordered porous structure, which created enhanced electrocatalytic properties over commercial RuO₂ nanoparticles for both oxygen and chlorine evolution reactions.

Keywords: ruthenium oxide; KIT-6; nanocasting; oxygen evolution reaction; chlorine evolution reaction

1. Introduction

The oxygen evolution reaction (OER) is an important core reaction for electrochemical energy conversion systems such as fuel cells, water splitting, and metal–air batteries [1,2]. The chlorine evolution reaction (CER) is also an essential reaction in the chlor–alkali process for the chemical industry, which uses chlorine as the main raw material. [3]. RuO₂ is considered as a highly active metal oxide material for both the OER and CER [4,5]. However, RuO₂ has the fatal problem of a very high unit price due to low reserves. Therefore, many research techniques have been developed to reduce its usage by enhancing its electrocatalytic properties [6–9]. Among these techniques, nanocasting is a facile and versatile structure design technique for synthesizing various nanostructures through replication of the microporous or mesoporous siliceous or non-siliceous materials for use as hard or soft templates. The nanocasting technique is a process by which the structure of the replicate can be obtained by filling the pores of the template with a metal precursor, followed by optional treatment and final removal of the template [10–13]. In this work, we demonstrate a structurally controlled ordered mesoporous RuO₂ replica through the nanocasting technique with mesoporous KIT-6 silica material as a template; the results reveal highly enhanced electrocatalytic activity and stability for OER and CER over commercial RuO₂ nanoparticles.

2. Results and Discussion

Figure 1a–c show representative transmission electron microscopy (TEM) and high-resolution TEM (HRTEM) images of the KIT-6 template. These images display a well-ordered mesoporous KIT-6 structure. Figure 1d shows the small-angle X-ray scattering (SAXS) pattern of the KIT-6 in

the range of $2\theta = 0.3\text{--}5.0^\circ$. Characteristic peaks of the crystalline KIT-6 phase (211), (220) and (332) planes appeared at 0.9° , 1.04° and 1.71° , respectively. This SAXS result can be assigned to a cubic ordered three-dimensional $Ia\bar{3}d$ symmetry structure [14,15], indicating that the obtained KIT-6 template has a well-ordered pore structure. The mesoporous properties of KIT-6, namely the pore-volume (0.975 cc g^{-1}), the pore size (9.056 nm) and the surface area ($868.3\text{ m}^2\text{ g}^{-1}$), were revealed by a nitrogen adsorption–desorption isotherm (Figure 1e).

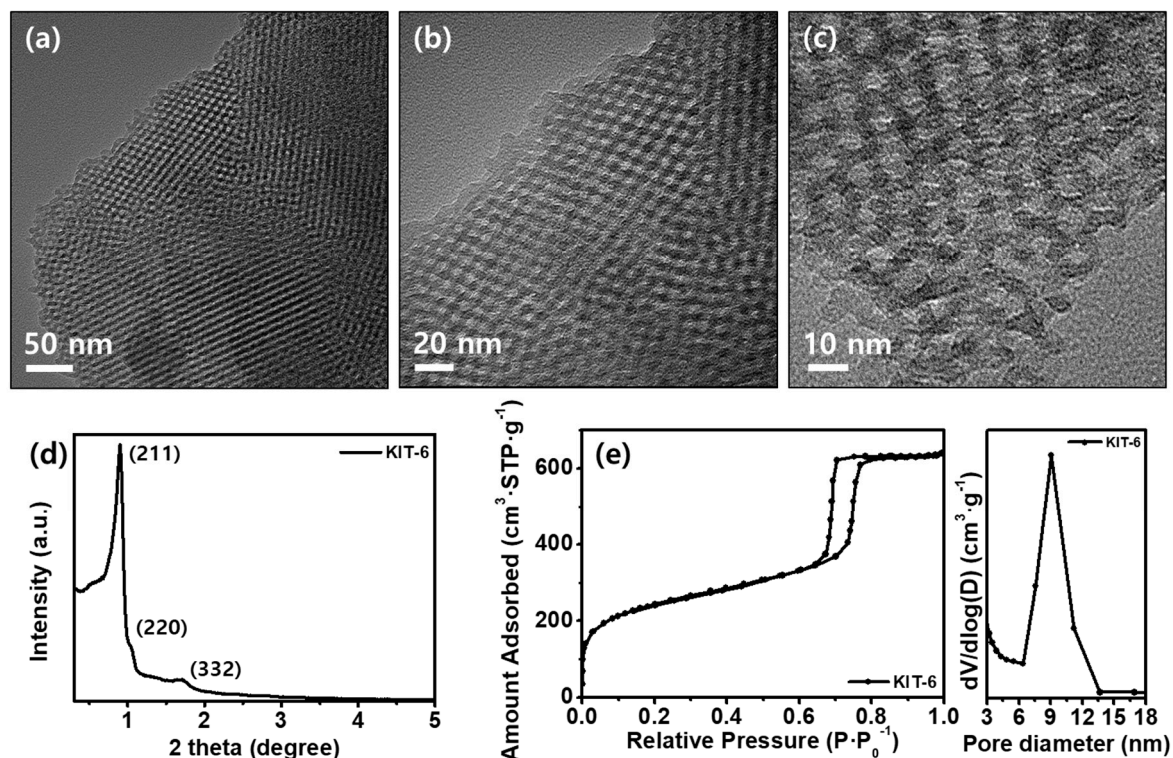


Figure 1. (a) TEM image, (b and c) HRTEM images, (d) SAXS pattern and (e) nitrogen adsorption–desorption isotherm (right: pore size distribution) of the KIT-6.

Figure 2 compares the structural properties of the structure-controlled (SC) RuO_2 obtained using the KIT-6 template and the commercial RuO_2 (Figure 2). Unlike RuO_2 , which shows an aggregated spherical particle structure with a particle size of about 26 nm in TEM and HRTEM images (Figure 2a), SC RuO_2 shows the shape of a framework structure and the same cubic symmetry as the KIT-6 template (Figure 2b). Furthermore, the particle wall thickness of SC RuO_2 is almost the same as the pore size of the KIT-6 template (KIT-6 pore size: 9.056 nm and particle wall thickness of SC RuO_2 : approximately 9 nm). The X-ray diffraction (XRD) patterns of both SC RuO_2 and commercial RuO_2 (Figure 2c) exhibit a crystalline phase of RuO_2 (JCPDS No. 43-1027).

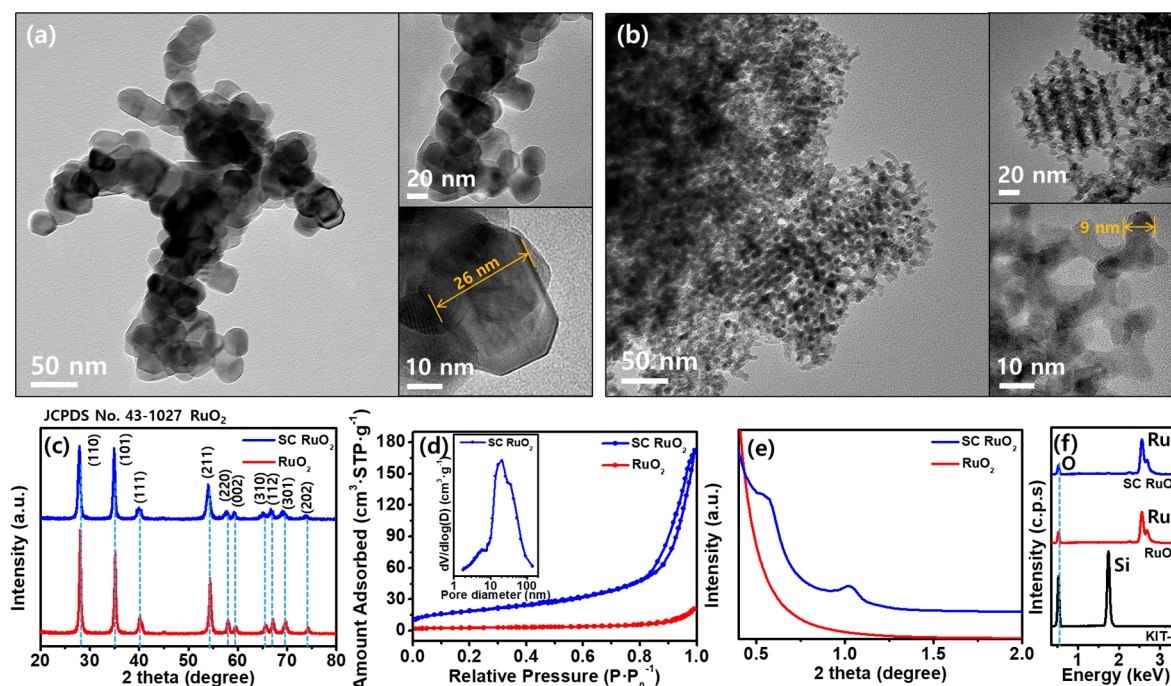


Figure 2. TEM and HRTEM image of (a) RuO₂ and (b) structure-controlled (SC) RuO₂. (c) XRD patterns, (d) nitrogen adsorption–desorption isotherm (inset: pore size distribution of SC RuO₂), (e) SAXS patterns of RuO₂ and SC RuO₂. (f) EDS spectra of KIT-6, RuO₂ and SC RuO₂.

To confirm the mesoporosity and long-range pore order of SC RuO₂, nitrogen adsorption–desorption isotherm and SAXS analysis were performed, respectively. SC RuO₂ possesses a typical mesoporosity with a type IV isotherm hysteresis loop [16] and a pore size between 2 nm and 50 nm (SC RuO₂: 20.7 nm), while RuO₂ exhibits nonporous properties (Figure 2d). It is noteworthy that the surface area of SC RuO₂ (69.1 m² g^{−1}) is seven times higher than that of RuO₂ (9.5 m² g^{−1}). In SAXS patterns (Figure 2e), only SC RuO₂ shows two typical peaks of the long-range pore order properties between 2θ = 0.5° and 1.0° [17]. Through energy dispersive X-ray spectrometer (EDS) analysis (Figure 2f), we confirmed that the KIT-6 was completely removed in the SC RuO₂ material.

The electrochemical analyses (linear sweep voltammetry (LSV), electrochemical impedance spectroscopy (EIS) and chronoamperometry (CA)) for OER and CER over the prepared catalysts were performed in a 0.5 M H₂SO₄ solution and a 5 M NaCl + 0.01 M HCl solution, respectively (Figure 3). LSV analyses were performed at a scan rate of 10 mV s^{−1} for OER (Figure 3a) and CER (Figure 3b) to estimate the electrocatalytic activities. Even though the onset potentials were the same for each catalyst (1.2 V and 1.1 V vs. Ag/AgCl for OER and CER, respectively), the peak current density of SC RuO₂ for OER was 272.7 mA cm^{−2}, which is 1.77 times higher than that of RuO₂ (154.1 mA cm^{−2}). In addition, the current density of SC RuO₂ for CER reached 616.4 mA cm^{−2}, which is 1.75 times higher than that of RuO₂ (352.1 mA cm^{−2}). EIS analysis was also performed at a constant voltage of 1.2 V for OER and 1.1 V for CER at frequencies from 100 kHz to 0.1 Hz with an amplitude of 5 mV to compare the charge transport ability between SC RuO₂ and RuO₂ during the OER (Figure 3c) and CER (Figure 3d). In the Nyquist plot, the quasi-semicircle is related to the Faradaic reactions at the electrode surface, and the diameter refers to the charge transfer resistance (R_{ct}) [18,19].

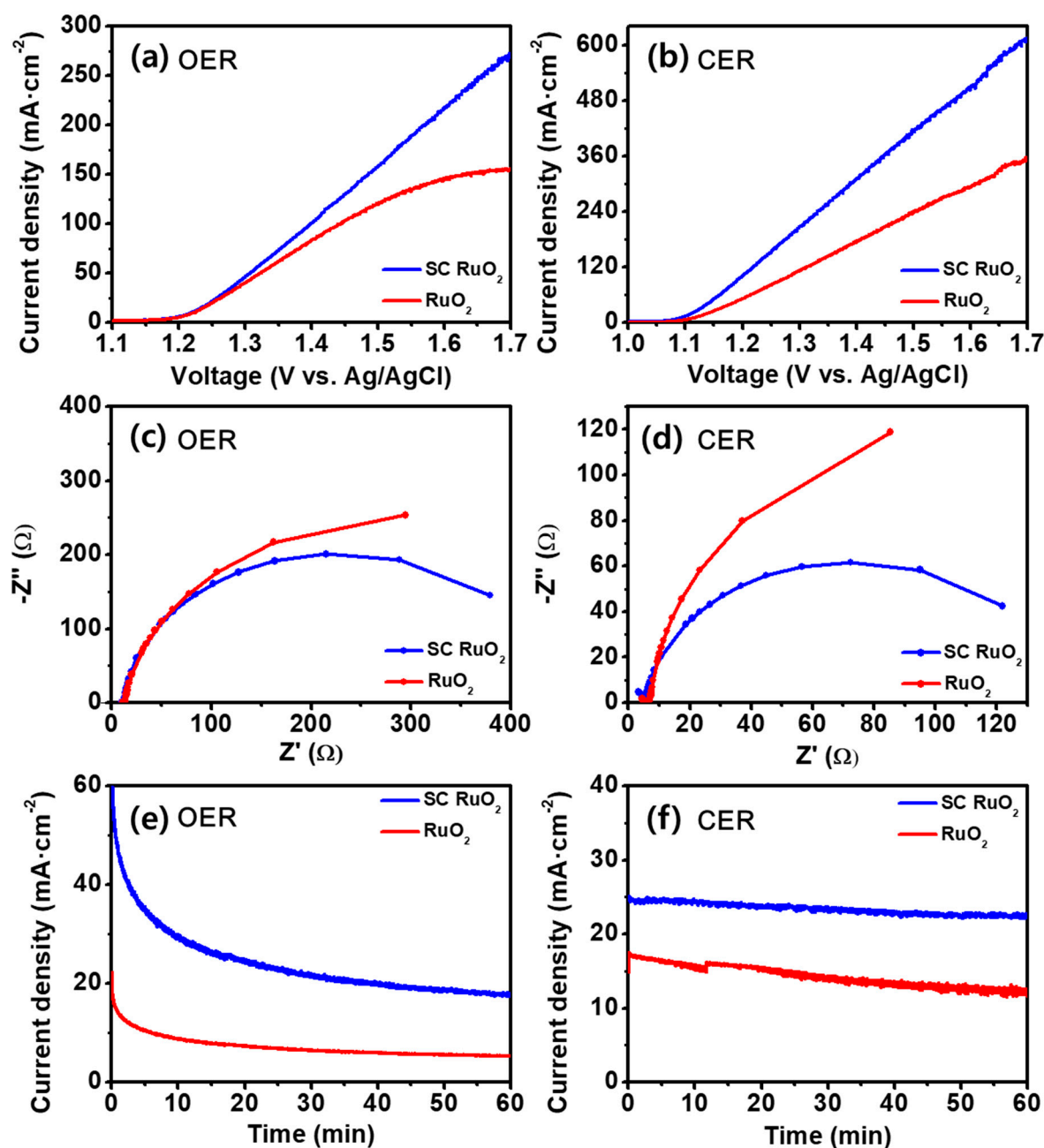


Figure 3. (a,c,e) OER in a 0.5 M H₂SO₄ solution and (b, d and f) CER in a 5 M NaCl + 0.01 M HCl solution over SC RuO₂ and RuO₂. (a,b) LSV curves at a scan rate of 10mV s⁻¹. Nyquist plots at a constant voltage of (c) 1.2 V and (d) 1.1 V at frequencies from 100 kHz to 0.1 Hz with an amplitude of 5 mV. CA curves at a constant voltage of (e) 1.25 V and (f) 1.15 V.

In both reactions, the Nyquist plots obtained via EIS analysis show smaller semicircles for SC RuO₂ than for RuO₂, which is related to the enhanced charge transfer ability of SC RuO₂. The obtained electrolyte resistance (R_s) and the R_{ct} for OER (R_s : 11.2 Ω, R_{ct} : 430.6 Ω) and CER (R_s : 5.1 Ω, R_{ct} : 144.9 Ω) of SC RuO₂ were lower than those of RuO₂ (R_s : 12.0 Ω, R_{ct} : 589.4 Ω for OER and R_s : 6.1 Ω, R_{ct} : 170.9 Ω for CER). Finally, CA tests were performed to examine the stability of SC RuO₂ and RuO₂ during OER and CER. Constant voltages of 1.25 V and 1.15 V vs. Ag/AgCl for the OER and CER, respectively, were applied for 60 min. As Figure 3e,f show, the current density of the OER and CER remains higher than that of SC RuO₂ during the reaction time, which suggests that the SC RuO₂ catalyst has high stability in both reactions. These electrochemical property results suggest that the potential

for initiating each reaction is the same due to the same constituent elements in both RuO₂ catalysts, but the reaction rate and the stability of the SC RuO₂ are much better than that of the RuO₂ because of the distinct structural properties of SC RuO₂, namely, its high surface area and mesoporosity.

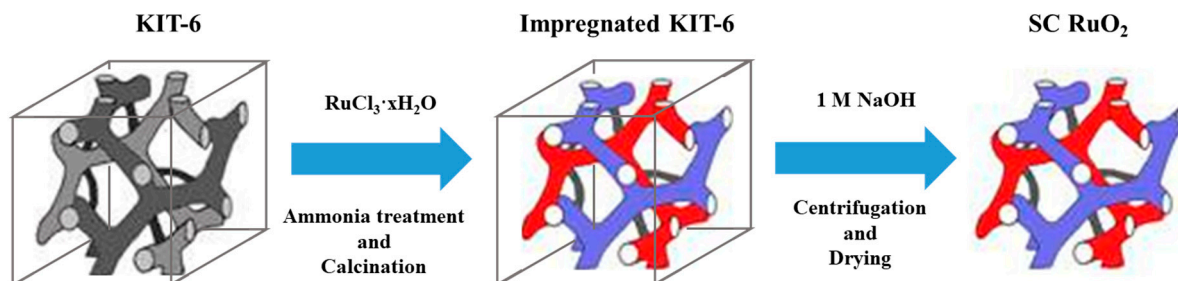
3. Materials and Methods

3.1. Synthesis of KIT-6 Nanoparticles

Mesoporous silica KIT-6 nanoparticles were prepared following a reported study in the literature [20]. Pluronic P123 (33.8 g, Aldrich, Saint Louis, MO, USA) was dissolved in distilled water (1220 mL), and hydrochloric acid (54.2 mL, 35%, Aldrich, Saint Louis, MO, USA) and 1-butanol (45.9 mL, Aldrich, Saint Louis, MO, USA) were added. Then, 92.8 mL of tetraethyl orthosilicate (TEOS, 98%, ACROS, Belgium) was added and the mixture was continuously stirred at 35 °C for 24 h. The final mixture was heated at 100 °C for 24 h. The white solid product was obtained by filtration and calcined at 550 °C for 6 h in air.

3.2. Preparation of Structure-Controlled RuO₂ (SC RuO₂) Catalyst

The replication process of the SC RuO₂ from KIT-6 as a template is depicted in Scheme 1. The replica was prepared by an incipient wetness impregnation (IWI) method using a RuCl₃·xH₂O precursor (Aldrich, Saint Louis, MO, USA) and as-prepared KIT-6. The ruthenium precursor (1.09 g) was dissolved in 10 mL of ethanol. This mixture was infused into 0.3 g of KIT-6. After the ethanol was evaporated, the sample was exposed to 28% ammonia vapor at 60 °C and calcined at 500 °C for 3 h [21]. After being calcined, the obtained powder was added to a 1 M NaOH solution to remove the KIT-6 template. The template-free product was collected by centrifugation, washed with distilled water and dried at 60 °C.



Scheme 1. Replication process for synthesizing SC RuO₂ by the nanocasting technique using KIT-6 nanoparticles.

3.3. Characterization

The crystal structure was characterized by SAXS (Rigaku, SmartLab, Japan) and an XRD (Rigaku, Ultima IV, Japan) equipped with a 2D detector (Hypix-3000) using Cu K-alpha ($\lambda = 0.154$ nm, 1.5401 Å). HRTEM (TECNAL, G2 T-20S, Japan) equipped with an EDS was used to verify the structural morphology and elemental composition of the prepared catalysts. Nitrogen adsorption–desorption analysis was conducted at 77 K using a physical adsorption instrument (Micromeritics, ASAP 2020, Norcross, GA, USA). To calculate the apparent surface area and the pore size distributions, the Brunauer–Emmett–Teller (BET) method and the Barret–Joyner–Halenda (BJT) theory were used, respectively. Electrochemical properties were investigated using LSV, EIS and CA techniques. These electrochemical analyses were carried out using a three electrode half-cell system connected to a potentiostat (ZIVE MP2A, WonATech, Seoul, Korea). A glassy carbon (0.196 cm²), an Ag/AgCl (1 M KCl) and a Pt wire (diameter: 0.5 mm, length: 50 mm, surface area: 0.7 cm²) were used as a working electrode, a reference electrode and a counter electrode, respectively. The catalysts were mixed with a 5 wt% Nafion solution (catalyst: Nafion = 90:10 wt%) and loaded onto the glassy carbon electrode (0.2 mg cm⁻¹).

4. Conclusions

In this study, we successfully synthesized a well-ordered mesoporous SC RuO₂ catalyst via a nanocasting technique using a KIT-6 template. SC RuO₂ exhibited highly improved electrocatalytic properties in terms of both activity and stability for the oxygen and chlorine evolution reactions over the commercial RuO₂ catalyst. The improved electrochemical performance of SC RuO₂ could be attributed to the following unique structural features: (i) well-distributed pores could promote electrolyte permeability for faster reactant migration, and (ii) framework structures with thin walls could accelerate electrocatalytic reactions by enlarging the surface area.

Author Contributions: J.H. conducted electrochemical analyses and contributed to the writing of the original manuscript. H.J.A. and T.-W.K. contributed to the synthesis of catalysts. K.-Y.L. and H.J.K. contributed to the physicochemical characterizations of catalysts. Y.K. and H.-J.C. designed and supervised the research.

Acknowledgments: This work was supported by the C1 Gas Refinery Program through a grant from the National Research Foundation of Korea (NRF) funded by the Ministry of Science and ICT (2016M3D3A1A01913251). This work was also supported by the flagship KRICT project (SI1911-50) from the Korea Research Institute of Chemical Technology.

Conflicts of Interest: The authors declare no conflict of interest.

References

1. Tahir, M.; Pan, L.; Idrees, F.; Zhang, X.; Wang, L.; Zou, J.-J.; Wang, Z.L. Electrocatalytic oxygen evolution reaction for energy conversion and storage: A comprehensive review. *Nano. Energy* **2017**, *37*, 136–157.
2. Delgado, D.; Minakshi, M.; McGinnity, J.; Kim, D.-J. Co/Mo bimetallic addition to electrolytic manganese dioxide for oxygen generation in acid medium. *Sci. Rep.* **2015**, *5*, 15208. [[CrossRef](#)] [[PubMed](#)]
3. Hansen, H.A.; Man, I.C.; Studt, F.; Abild-Pedersen, F.; Bligaard, T.; Rossmeisl, J. Electrochemical chlorine evolution at rutile oxide (110) surfaces. *Phys. Chem. Chem. Phys.* **2010**, *12*, 283–290. [[CrossRef](#)] [[PubMed](#)]
4. Exner, K.S.; Anton, J.; Jacob, T.; Over, H. Controlling selectivity in the chlorine evolution reaction over RuO₂ based catalysts. *Angew. Chem. Int. Ed.* **2014**, *53*, 11032–11035. [[CrossRef](#)] [[PubMed](#)]
5. Reier, T.; Oezaslan, M.; Strasser, P. Electrocatalytic oxygen evolution reaction (OER) on Ru, Ir, and Pt catalysts: A comparative study of nanoparticles and bulk materials. *ACS Catal.* **2012**, *2*, 1765–1772. [[CrossRef](#)]
6. Xiong, K.; Peng, L.; Wang, Y.; Liu, L.; Deng, Z. In situ growth of RuO₂-TiO₂ catalyst with flower-like morphologies on the Ti substrate as a binder-free integrated anode for chlorine evolution. *J. Appl. Electrochem.* **2016**, *46*, 841–849. [[CrossRef](#)]
7. Nazir, R.; Basak, U.; Pande, S. Synthesis of one-dimensional RuO₂ nanorod for hydrogen and oxygen evolution reaction: An efficient and stable electrocatalyst. *Colloids. Surf. A.* **2019**, *560*, 141–148. [[CrossRef](#)]
8. Panic, V.V.; Dekanski, A.B.; Mitric, M.; Milonjic, S.K.; Miskovic-Stankovic, V.B.; Nikolic, B.Z. The effect of the addition of colloidal iridium oxide into sol-gel obtained titanium and ruthenium oxide coatings on titanium on their electrochemical properties. *Phys. Chem. Chem. Phys.* **2010**, *12*, 7521–7528. [[CrossRef](#)]
9. Petrykin, V.; Macounová, K.; Okube, M.; Mukerjee, S.; Krtil, P. Local structure of Co doped RuO₂ nanocrystalline electrocatalytic materials for chlorine and oxygen evolution. *Catal. Today.* **2013**, *202*, 63–69. [[CrossRef](#)]
10. Lu, A.-H.; Schüth, F. Nanocasting: A versatile strategy for creating nanostructured porous materials. *Adv. Mater.* **2006**, *18*, 1793–1805. [[CrossRef](#)]
11. Schüth, F. Non-siliceous mesostructured and mesoporous materials. *Chem. Mater.* **2001**, *13*, 3184–3195. [[CrossRef](#)]
12. Gu, D.; Schüth, F. Synthesis of non-siliceous mesoporous oxides. *Chem. Soc. Rev.* **2014**, *43*, 313–344. [[CrossRef](#)] [[PubMed](#)]
13. Ren, Y.; Ma, Z.; Bruce, P.G. Ordered mesoporous metal oxides: synthesis and applications. *Chem. Soc. Rev.* **2012**, *41*, 4909–4927. [[CrossRef](#)] [[PubMed](#)]
14. Suzuki, N.; Kiba, S.; Yamauchi, Y. Fabrication of mesoporous silica KIT-6/polymer composite and its low thermal expansion property. *Mater. Lett.* **2011**, *65*, 544–547. [[CrossRef](#)]
15. Kleitz, F.; Choi, S.H.; Ryoo, R. Cubic *la3d* large mesoporous silica: synthesis and replication to platinum nanowires, carbon nanorods and carbon nanotubes. *Chem. Commun.* **2003**, *17*, 2136. [[CrossRef](#)]

16. Grewe, T.; Deng, X.; Tüysüz, H. A Study on the growth of Cr₂O₃ in ordered mesoporous silica and its replication. *Chem. Eur. J.* **2014**, *20*, 7692–7697. [[CrossRef](#)] [[PubMed](#)]
17. Kim, T.-W.; Solovyov, L.A. Synthesis and characterization of large-pore ordered mesoporous carbons using gyroidal silica template. *J. Mater. Chem.* **2006**, *16*, 1445–1455. [[CrossRef](#)]
18. Verma, M.L.; Minakshi, M.; Singh, N.K. Synthesis and characterization of solid polymer electrolyte based on activated carbon for solid state capacitor. *Electrochim. Acta.* **2014**, *137*, 497–503. [[CrossRef](#)]
19. Verma, M.L.; Minakshi, M.; Singh, N.K. Structural and electrochemical properties of nanocomposite polymer electrolyte for electrochemical devices. *Ind. Eng. Chem. Res.* **2014**, *53*, 14993–15001. [[CrossRef](#)]
20. Kim, T.-W.; Kleitz, F.; Paul, B.; Ryoo, R. MCM-48 like large mesoporous silicas with tailored pore structure: facile synthesis domain in a ternary triblock copolymer-butanol-water system. *J. Am. Chem. Soc.* **2005**, *127*, 7601–7610. [[CrossRef](#)]
21. Cui, X.; Zhou, J.; Ye, Z.; Chen, H.; Li, L.; Ruan, M.; Shi, J. Selective catalytic oxidation of ammonia to nitrogen over mesoporous CuO/RuO₂ synthesized by co-nanocasting-replication method. *J. Catal.* **2010**, *270*, 310–317. [[CrossRef](#)]



© 2019 by the authors. Licensee MDPI, Basel, Switzerland. This article is an open access article distributed under the terms and conditions of the Creative Commons Attribution (CC BY) license (<http://creativecommons.org/licenses/by/4.0/>).